Nonlinear Analysis of the Colpitts Oscillator and Applications to Design

Gian Mario Maggio, *Student Member, IEEE*, Oscar De Feo, and Michael Peter Kennedy, *Fellow, IEEE*

***Abstract*—This paper reports a methodological approach to the analysis and design of sinusoidal oscillators based on bifurcation analysis. The simple Colpitts oscillator is taken as an example to demonstrate this nonlinear approach for both the nearly sinusoidal and chaotic modes of operation. In particular, it is shown how regular and irregular (chaotic) oscillations can be generated, depending on the circuit parameters.**

***Index Terms*— Bifurcations, chaos, coexistence of solutions, Colpitts oscillator, continuation methods.**

I. Introduction

THE aim of this paper is to show how bifurcation analysis can be employed as a tool for designing oscillators in order to obtain either a nearly sinusoidal oscillation or chaotic behavior.

Bifurcation analysis has already been used in the past, albeit implicitly, in the design of oscillators. In fact, in most sinusoidal oscillator configurations, the oscillation condition coincides with the Hopf bifurcation condition: usually a supercritical bifurcation for which an equilibrium point loses its stability and a stable limit cycle is generated [1]. Moreover, the locus of the first period-doubling bifurcation in parameter space is often computed with harmonic balance methods [2]–[4], in order to bound the region of nearly sinusoidal behavior.

Today, with a view to developing design techniques for chaos generation, there is a definite need to characterize the complex behavior exhibited by oscillators for some combinations of the circuit parameters. From this perspective, it should be noted that by moving the control parameters away from the oscillation condition many different kinds of complex behavior may arise. These include chaotic behavior or even more complex situations associated with coexisting attractors.

While a huge research effort has been invested in the last decade in the investigation of chaotic dynamics, the specialized literature does not report much about the implications of the coexistence of different attractors. The latter phenomenon can indeed be significant in applications. In practice, the coexistence of attractors implies that trajectories starting close to an attractor may suddenly jump (catastrophically) to a different attractor. Even more intriguing is the situation in which coexisting attractors possess fractal or intermingled basin of attractions. In this case, due to physical noise, the observed signal may be the result of a random switching of the system trajectory between two or more attractors.

On the other hand, with the aim of characterizing the statistical properties of the signal generated, it is useful to classify the chaotic signal depending on the mechanism which led to chaos. In fact, the spectrum of a chaotic signal can vary significantly, depending on the principal mechanism governing its dynamics; for instance, whether it is the result of a classical Feigenbaum cascade or if it is associated with a Shil'nikov homoclinic loop.

In this work we consider the Colpitts oscillator as a paradigm for sinusoidal oscillation, with the aim of drawing some general conclusions about the design of this type of oscillator. The motivations for considering this circuit are many, including the following.

- The Colpitts oscillator is a single-transistor implementation of a sinusoidal oscillator which is widely used in electronic devices and communication systems.
- The frequency of operation can vary from a few hertz up to the microwave region (gigahertz), depending on the technology.
- The system possesses an intrinsic nonlinearity given by the exponential characteristic of the active device.
- The system is nonsymmetric and therefore generic.
- The Colpitts oscillator exhibits rich dynamical behavior like many other third-order oscillator configurations analyzed in the literature [5]–[7]. In particular, for the Colpitts oscillator there is extensive numerical and experimental evidence of chaotic behavior [8]–[10].

The approach that we will follow in our analysis is in the context of the qualitative theory of nonlinear dynamical systems [11], [12]. We emphasize that, in general, nonlinear dynamical systems cannot be solved analytically. In many cases, extensive simulations have been used to study numerically the behavior of these systems. However, in many applications it is not sufficient to look at a single trajectory. Usually a large amount of computer time is required to gain a more general (but often incomplete) idea of the behavior of a system. Hence, the importance of qualitative analysis.

Manuscript received November 3, 1998; revised March 23, 1999. The work of G. M. Maggio and M. P. Kennedy was supported in part the European Union under Grant ERBFMBICT950310, and in part by the Forbairt International Collaboration Programme under Grant IC/98/052. The work of O. De Feo was supported in part by the Swiss National Science Foundation under Grant 20-47 172.96. This paper was recommended by Associate Editor V. P. Villar.

G. M. Maggio is with the Institute of Nonlineaar Science, University of California, San Diego 92093-0402 USA.

M. P. Kennedy is with the Department of Electronic and Electrical Engineering, University College Dublin, Dublin 4, Ireland.

O. De Feo is with the Department of Electrical Engineering, Swiss Federal Institute of Technology (EPFL), Lausanne, Switzerland.

Publisher Item Identifier S 1057-7122(99)07227-X.

In particular, we are interested in the qualitative analysis of time-invariant sets in the state space. Examples of these invariant sets include steady states, periodic solutions, and strange attractors.

Qualitative analysis is concerned mainly with the investigation of the stability of the invariant sets with respect to small perturbations, and their dependence on the model parameters. In particular, a bifurcation occurs when there exists a perturbation such that the invariant set exhibits different qualitative properties. Thus, the qualitative analysis of a dynamical system can lead to the analysis of the bifurcation that the system undergoes, as the control parameters are varied.

For the Colpitts oscillator, by making use of bifurcation analysis and other nonsimulative techniques (in contrast with linear analysis and numerical time-domain simulations), we illustrate how a complete picture of the dynamical behavior of the circuit as a function of its parameters can be obtained. In particular, we show how regular and irregular (chaotic) oscillations can be generated and how the parameter space is organized in terms of local and global bifurcations.

The paper's structure is as follows. In Section II we introduce the circuit model for the Colpitts oscillator. We illustrate its dynamical behavior in Section III. In Section IV we introduce continuation methods (versus simulation) in order to carry out a bifurcation analysis of the system. The results of the bifurcation analysis for the sinusoidal and the highly nonlinear regions of operation of the Colpitts are presented in Sections V and VI, respectively. In Section VII we discuss a robustness analysis of the circuit model. Finally, design aspects are outlined in Section VIII.

II. Colpitts Oscillator

A. Circuit Model

We consider the classical configuration of the Colpitts oscillator containing a bipolar junction transistor (BJT) as the gain element and a resonant network consisting of an inductor and a pair of capacitors, as illustrated in Fig. 1(a). Note that the bias is provided by the current source I_0, characterized by a Norton-equivalent conductance G_0.

According to the qualitative theory in nonlinear dynamics, we select a *minimal* model for the circuit. The idea here is to consider as simple a circuit model as possible which maintains the essential features exhibited by the real Colpitts oscillator. This requires of course an *a posteriori* robustness analysis of the model in order to validate the results. In fact, as was already pointed out, a rigorous (even if numerically supported) bifurcation analysis of a simpler model can provide much more insight than extensive simulations of a more complete circuit model.

Namely, we make the following simplifying hypotheses.

1) *(H.1)* Ideal bias circuit, i.e., the bias current on the emitter (E) is provided by an ideal current source, I_0, with $G_0 = 0$.
2) *(H.2)* Ideal linear passive and reactive elements;
3) *(H.3)* The transistor T is modeled simply by a (voltage-controlled) nonlinear resistor R_E and a linear current-controlled current source, as shown in Fig. 1(b). Moreover, the following applies.

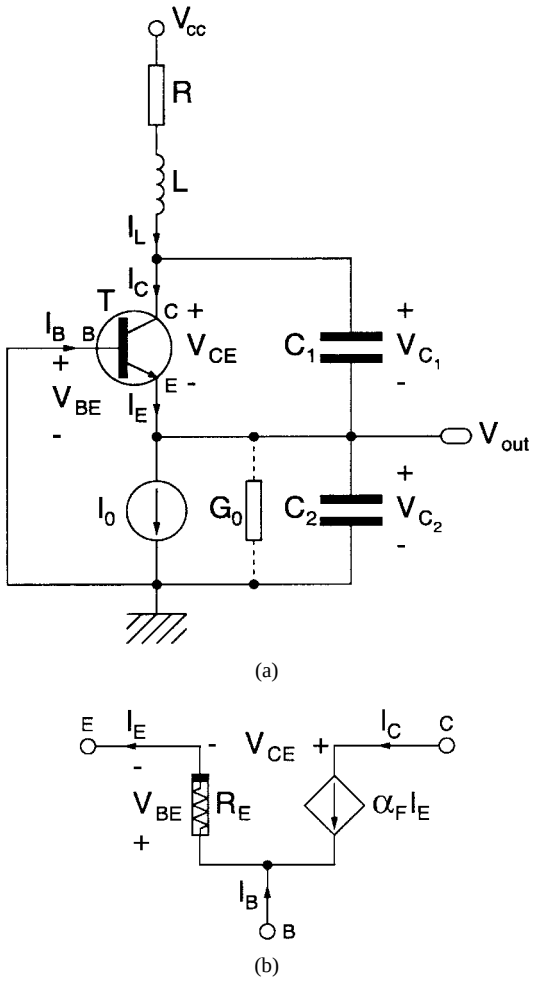

Fig. 1. Circuit model: (a) Schematic of the Colpitts oscillator. (b) BJT transistor model in common base configuration.

a) *(H.3a)* We model the *V–I* characteristic of R_E with an exponential function, namely

$$I_E = Is\left[\exp\left(\frac{V_{BE}}{VT}\right) - 1\right] \approx I_s\left[\exp\left(\frac{V_{BE}}{VT}\right)\right], \qquad \text{if } V_{BE} \gg V_T \tag{1}$$

where I_s is the inverse saturation current and $V_t \simeq 26$ mV at room temperature.

b) *(H.3b)* We assume $\alpha_F = 1$ where α_F is the common-base forward short-circuit current gain. This corresponds to neglecting the base current.

c) *(H.3c)* Parasitic dynamics of the transistor are neglected.[1]

We emphasize that the key element in the transistor model is the nonlinear resistor (modeling the B-E junction) which is responsible for most of the phenomena illustrated in this work. The neglected elements have only a scaling effect on the observed behavior. In other words, more complete models do

[1] Note that the parasitic capacitors C_{be} and C_{ce} add in parallel with C_2 and C_1, respectively.

not affect the qualitative dynamics of the circuit, as discussed in Section VII, only their position in the parameter space.

B. State Equations

The state equations for the schematic in Fig. 1(a) are the following:

$$\begin{aligned} C_1\frac{dV_{C_1}}{dt} &= -f(V_{C_2}) + I_L \\ C_2\frac{dV_{C_2}}{dt} &= I_L - I_0 \\ L\frac{dI_L}{dt} &= -V_{C_1} - V_{C_2} - RI_L + V_{CC} \end{aligned} \tag{2}$$

where $f(\cdot)$ is the driving-point characteristic of the nonlinear resistor. This characteristic can be expressed in the form $I_E = f(V_{C_2}) = f(-V_{BE})$ and, in particular, from (1) it follows that

$$f(V_{C_2}) = I_S \exp\left(-\frac{V_{C_2}}{V_T}\right)$$

C. Normalization and Parameters

We now introduce a set of dimensionless state variables (x_1, x_2, x_3) and we choose the operating point of (2) to be the origin of the new coordinate system. In particular, we normalize voltages, currents, and time with respect to $V_{\text{ref}} = V_t$, $I_{\text{ref}} = I_O$, and $t_{\text{ref}} = 1/\omega_0$, respectively, where $\omega_0 = 1\sqrt{L(C_1C_2/C_1 + C_2)}$ is the resonant frequency of the unloaded L-C tank circuit.

The state equations (2) of the Colpitts oscillator can then be rewritten in the form

$$\begin{pmatrix} \dot{x}_1 \\ \dot{x}_2 \\ \dot{x}_3 \end{pmatrix} = \begin{pmatrix} \dfrac{g^*}{Q(1-k)}[-n(x_2) + x_3] \\ \dfrac{g^*}{Qk}x_3 \\ -\dfrac{Qk(1-k)}{g^*}[x_1 + x_2] - \dfrac{1}{Q}x_3 \end{pmatrix} \tag{3}$$

where

$$n(x_2) = \exp(-x_2) - 1$$

and $k = C_2/(C_1 + C_2)$.

Note the remarkable simplicity of the (smooth) nonlinearity of the model. Indeed, in system (3), only the first equation contains the nonlinear term $n(x_2)$ which, in turn, depends only on one of the state variables, namely x_2. Also, it should be noted that the dynamical behavior of the system (3) depends only on the following two parameters:

- g^*, the loop gain of the oscillator;
- $Q = (\omega_0 L/R)$, the quality factor of the (unloaded) tank circuit,

while k has just a scaling effect on the state variables.

The parameter g^* represents the (open) loop gain of the oscillator when the phase condition of the Barkhausen criterion [13] is satisfied. We will show in Section V that a (supercritical) Hopf bifurcation occurs at $g^* = 1$, giving birth to a nearly-sinusoidal oscillation.

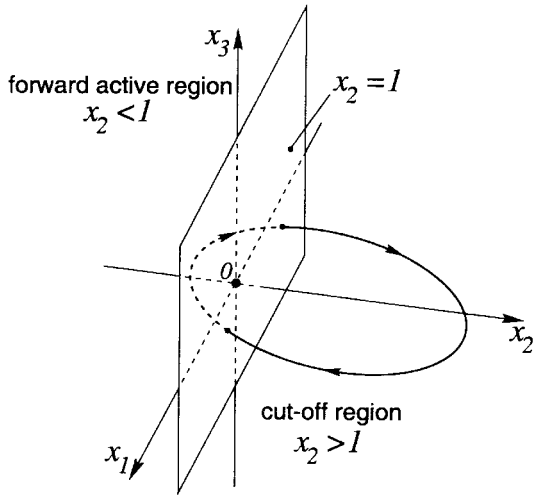

Fig. 2. Sketch of the working principle of the Colpitts oscillator in the state space. The trajectory is accelerated in the forward active region of the active device but evolves freely, according to the natural mode of the resonant circuit, in the cut off region of operation.

III. Dynamical Behavior

A. State Space Representation

In Fig. 2, we show the (normalized) state space (x_1, x_2, x_3) associated with the Colpitts oscillator. The origin, which is the only equilibrium point of the system, corresponds to the operating point of the circuit. Moreover, the state space can be split into two distinct regions which correspond to the modes of operation of the BJT. Note that for $x_2 \leq 1$ the transistor works in its forward active region while for $x_2 > 1$ it is cut off.

The orbit sketched in Fig. 2 represents a limit cycle in state space corresponding to a nearly-sinusoidal oscillation. We can conceive a geometrical interpretation of this class-C mode of operation of the Colpitts oscillator. Namely, by drawing a mechanical analogy, in the forward active region the system trajectories are accelerated by the energy provided by the active device (BJT). On the other hand, in the cut-off region the trajectory evolves freely according to the natural mode of oscillation of the L-C network the unloaded$L$-C tank circuit. A more detailed description of the qualitative dynamics of the Colpitts oscillator, referring to a piecewise-linear model, is reported in [14].

B. Periodic Solutions

An example of an actual nearly-sinusoidal oscillation for the Colpitts oscillator is presented in Fig. 3(a) and (b) where projections of the state space and the time evolution $x_3(t)$ are shown, respectively.

In the sequel we will refer to this kind of orbit as the fundamental (nearly) sinusoidal solution of the Colpitts oscillator. This behavior is significantly different from the more complicated oscillations that the Colpitts oscillator can exhibit. In fact, for higher values of the loop gain g^*, the oscillations can deviate significantly from nearly sinusoidal behavior. Fig. 3(c) and (d) shows an example of such a complicated periodic orbit, for parameter values for which strong nonlinear effects predominate. From Fig. 3(c), we can observe that in this case the orbit in state space exhibits several oscillations

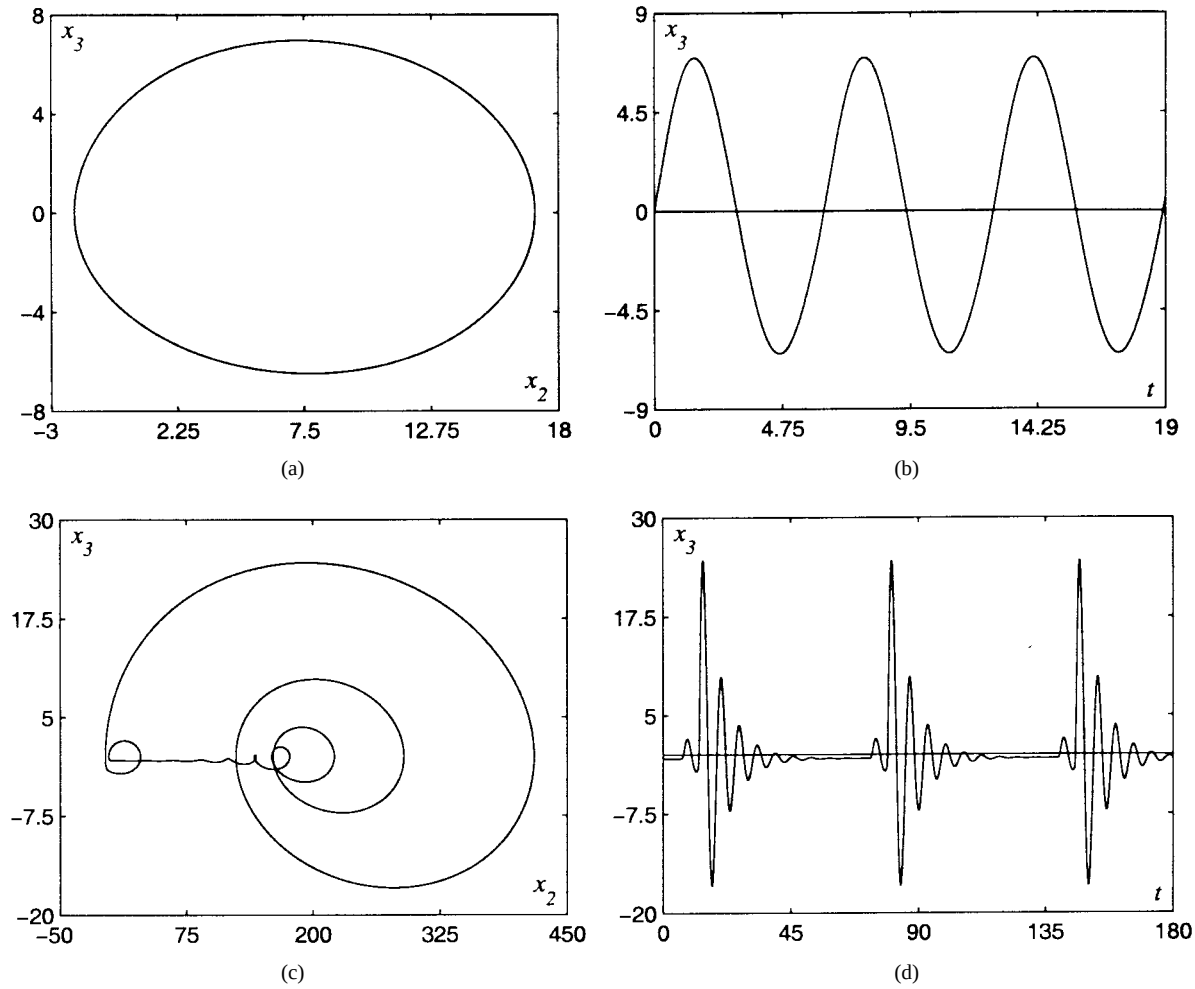

Fig. 3. The n-pulse families of periodic solutions for the Colpitts oscillator. Cycles belonging to different solution families differ in the number of oscillations in the cutoff region or, equivalently, in the number of pulses in the time series $x_3(t)$. The nearly sinusoidal cycle (1-pulse). (a) Projection of the limit cycle onto the (x_2, x_3) plane. (b) The corresponding time series of x_3. A six-pulse solution. (c) Projection of the limit cycle onto the (x_2, x_3) plane. (d) The corresponding time series of x_3.

in the cut-off region $(x_2 > 1)$ that manifest themselves as a sequence of pulses in the corresponding time series $x_3(t)$, as shown in Fig. 3(d).

Simulations of the circuit suggest that there exists an infinity of families of periodic solutions characterized by an increasing number of oscillations in the cut-off region.

A more detailed discussion about the solution families for the Colpitts oscillator will be presented in Section VI-A, where we will discuss the bifurcations of the limit cycles associated with each periodic solution.

C. Simulation Results

1) Bifurcation Diagram: Fig. 4(a) shows a simulated two-parameter bifurcation diagram illustrating the dependence of the dynamical behavior of the Colpitts oscillator on the two control parameters Q and g^*. This bifurcation diagram has been obtained by brute force time-domain simulation of the system throughout the parameter space (Q, g^*). The resulting trajectories are analyzed[2] in order to establish whether the system, at steady state, settles to an equilibrium point, a limit cycle, or a chaotic attractor.

In practice, for each parameter combination, the system is simulated by numerical integration for a sufficiently long time and the transient is discarded. The resulting attractor on a properly chosen Poincaré section $(x_2 = 1)$ is then analyzed by evaluating the distance between successive intersections and, finally, the period is estimated.

In Fig. 4(a) different behaviors are denoted by different gray levels. The white area indicates a period-one solution, like the one corresponding to a nearly-sinusoidal oscillation of the Colpitts oscillator, illustrated in Fig. 3(a) and (b). The darker regions correspond to orbits of increasing period. Finally, for the black area, no periodic behavior was detected, and so we associate chaotic behavior with the corresponding region.

In particular, from Fig. 4(a) we note the presence of a large region of complex behavior in the parameter space in which the system undergoes several bifurcations when varying either of the parameters g^* and Q. This is clearly visible in Fig. 4(b) which shows a one-parameter bifurcation diagram corresponding to the horizontal line segment $A \rightarrow B$ in Fig. 4(a). Feigenbaum period-doubling cascades,

[2]The algorithm to determine the dynamical behavior of the system was implemented using the C-library CHAOSLIB by A. Abel and C. Wegener (E-mail: wegener@vdp.ucd.ie).

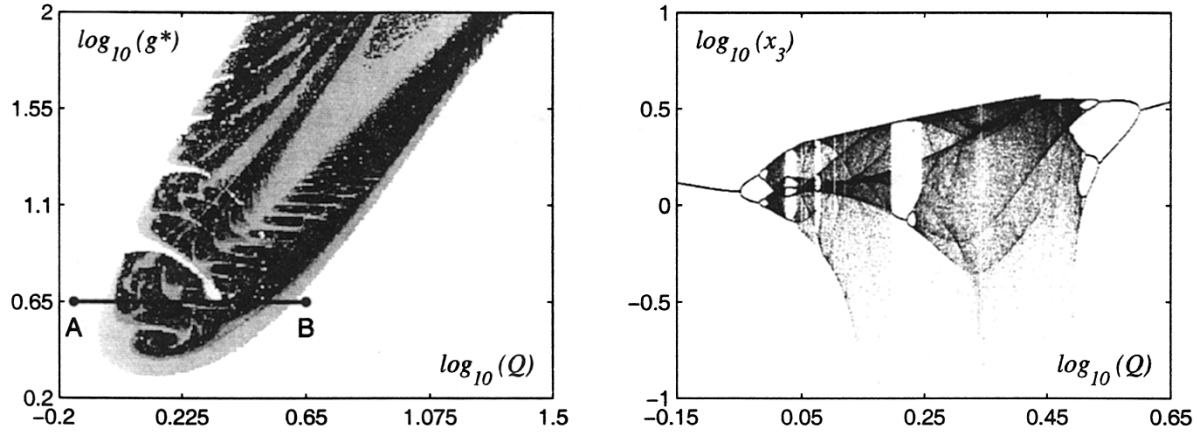

Fig. 4. Bifurcation diagrams (by simulation) for the Colpitts oscillator, obtained by analyzing the intersections of the system trajectory with the Poincaré section $x_2 = 1$. (a) Two-parameter bifurcation diagram illustrating the dependence of the orbit period on the parameters (Q, g^*). The white area corresponds to period-1 behavior, while darker areas correspond to more complex periodic and nonperiodic behavior. (b) One-parameter bifurcation diagram of x_3 versus Q, along the path $A \rightarrow B$ in Fig. 4(a) $(\log_{10} g^* = 0.6500)$.

chaotic regions, and periodic windows are clearly visible in Fig. 4(b).

2) Limitations of Simulation Methods: At this point in the discussion we would like to emphasize the limitations of simulation techniques.

First, it should be noted that the results shown so far depend on the choice of the Poincaré section adopted for carrying out the period classification. Namely, different Poincaré sections give rise to different diagrams, providing different kinds of information. It follows that simulation results may be only partial and sometimes misleading. Also, we remark that in Fig. 4(a) a change in color might correspond to a real bifurcation or to a jump to a coexisting attractor. It is impossible to distinguish between these different situations by relying only on the results of simulations.

In the next section we will discuss how to overcome such limitations through a computer assisted bifurcation analysis of the system and we will compare the results with those obtained by brute-force simulation.

IV. Bifurcation Analysis

A. Introduction

In this section we illustrate the methodology and the techniques employed for carrying out a bifurcation analysis of (our model of) the Colpitts oscillator.

In particular, we consider continuation techniques, instead of simulation, to perform bifurcation analysis. Continuation methods allow one to translate the bifurcation analysis of equilibria and cycles into the solution of an implicit algebraic equation which can be computed systematically. Hence, the bifurcation analysis is reduced to locating the zeroes of some functions, which can be found, with the desired precision, by using Newton-based algorithms.

B. Continuation Methods

Continuation methods permit the analysis of the dependence of system invariants (like equilibria or cycles) on the control parameters. Namely, given a dynamical system, for instance an ODE

$$\dot{x} = F(x;\mu), \quad x \in \mathbb{R}^n, \quad \mu \in \mathbb{R}^p$$

where x is the state vector and μ represents the parameter set, we are interested in how the qualitative properties of the system invariants change when we vary the parameters. For example, we might be interested in changes of the stability of an equilibrium point, depending on the parameters.

For certain invariants, namely equilibria and cycles, it is possible to express their existence in an algebraic implicit form of the kind

$$G(X) = 0$$

where X is a suitable space that, in general, is obtained by combining the control parameters, the state variables, and the dummy[3] variables [15]–[17].

The defining function G can be very simple (for equilibria)

$$G(X) = F(x;\mu), \quad X \equiv (x;\mu)$$

or incredibly complex (for cycles) and can be obtained by special procedures, such as collocation methods [15]. In the case of cycles the X space is constructed by extending the (x, μ) space with variables obtained from the discretization of the cycle itself.

However, the main point is that given an initial solution (e.g., an equilibrium or a cycle), by using an appropriate continuation algorithm (usually based upon prediction-correction methods for locating zeroes of functions) it is possible to vary one parameter μ_i and to follow the locus in the X space satisfying the condition $G(X) = 0$. In other words, this process consists of determining how the invariant moves and deforms with variations of one parameter. Furthermore, it is possible to monitor, along the continuation path, a certain number of so-called test functions [16] whose zeroes correspond to bifurcations of the invariants.

[3] Auxiliary variables used in the continuation process either for discretization or monitoring purposes.

There are several advantages to using continuation methods as opposed to simulation in systems analysis.

- The solutions can be followed in the parameter space even if they are unstable: by contrast, simulation allows the observation of stable solutions only. In this regard, it should be noted that unstable periodic orbits and, in particular saddles, are involved in many bifurcation phenomena. Furthermore, the saddles' invariants separate the basins of attraction of different attractors.
- There is no need to wait for transients to settle before studying the invariants.
- The results are independent of the choice of Poincaré section.
- Numerical problems associated with sensitivity to the initial conditions are avoided.
- Continuation makes it possible to detect hysteretic phenomena due to coexisting attractors. This is difficult to achieve by simulation methods.

C. Application to the Colpitts Oscillator

In this work we used the AUTO97 [18] and CONTENT [19] continuation packages for carrying out a bifurcation analysis of the Colpitts oscillator with respect to the parameters Q and g^*.

In particular, we distinguish between a sinusoidal region, i.e., the region of the parameter space where the oscillation of the Colpitts is nearly-sinusoidal, and a nonlinear region where strongly nonlinear effects predominate and the oscillation deviates significantly from sinusoidal behavior.

The sinusoidal region includes the area in the parameter space close to the locus $g^* = 1$ ($\Leftrightarrow \log_{10} g^* = 0$), where the Barkhausen criterion is satisfied. However, if the quality factor Q is high enough, the sinusoidal region can extend to relatively large values of the loop gain g^*. This will be discussed in more detail in Section VIII, where the parameter space will be characterized in terms of the total harmonic distortion (THD) of the signal generated.

V. SINUSOIDAL REGION

In this section we consider the nearly sinusoidal mode of operation of the Colpitts oscillator. In particular, we will show that, for the circuit model considered, the sinusoidal oscillation observed in the Colpitts oscillator is associated with a (supercritical) Hopf bifurcation.

A. Oscillation Condition

For the model of the Colpitts oscillator that we consider, application of the Barkhausen criterion provides the oscillation condition $g^* = 1$ ($\Leftrightarrow \log_{10} g^* = 0$). We now show that actually, for this model, a Hopf bifurcation occurs for $g^* = 1$. Correspondingly, the equilibrium point $O \equiv (0,0,0)$ admits a pair of pure imaginary eigenvalues $\pm \jmath \omega_H$.

To verify what we stated above, we consider the linearization (i.e., the Jacobian) of the vector field (3) at the equilibrium point O

$$A = J|_O = \begin{pmatrix} 0 & \dfrac{g^*}{Q(1-k)} & \dfrac{g^*}{Q(1-k)} \\ 0 & 0 & \dfrac{g^*}{Qk} \\ -\dfrac{Qk(1-k)}{g^*} & -\dfrac{Qk(1-k)}{g^*} & -\dfrac{1}{Q} \end{pmatrix}. \tag{4}$$

The corresponding characteristic equation, $\det(A - \lambda I) = 0$ is given by

$$\lambda^3 + \frac{1}{Q}\lambda^2 + \lambda + \frac{g^*}{Q} = 0. \tag{5}$$

By imposing $\lambda = \jmath \omega_H$ it follows that

$$\begin{cases} g^* &= 1 \\ \omega_H &= 1 \end{cases}$$

confirming that for $g^* = 1$ the equilibrium O of (3) is characterized by a pair of purely imaginary eigenvalues with unitary angular frequency (due to the normalization) $\lambda_{1,2} = \pm \jmath$. Substituting into (5) it follows also that $\lambda_3 = -1/Q$.

We now need to check the nondegeneracy conditions for the Hopf bifurcation [17]. Regarding the transversality condition, it can be readily verified that, for the Colpitts oscillator

$$\left(\frac{d\,\mathrm{Re}[\lambda_{1,2}]}{dg^*}\right)\bigg|_{g^*=1} > 0, \qquad \forall Q > 0$$

On the other hand, according to [17], the first Lyapunov coefficient, l_1, which determines whether the Hopf bifurcation is subcritical or supercritical turns out to be

$$l_1 = \frac{-1}{16}\,\frac{Q^5}{(1+4Q^2)(1+Q^2)^2}. \tag{6}$$

It follows that for the Colpitts oscillator: $l_1(Q) < 0, \forall Q > 0$. Hence, for the model considered, the Hopf bifurcation at $g^* = 1$ is always nondegenerate ($l_1 \neq 0$) and, in particular it is always supercritical, thus giving birth to a stable limit cycle.

VI. THE NONLINEAR REGION

In this section we illustrate the bifurcation phenomena occurring in the parameter region of the Colpitts oscillator where strongly nonlinear effects predominate, so that the behavior is far from sinusoidal.

A. Families of Solutions and Their Bifurcations

As was previously mentioned, the Colpitts oscillator admits different periodic solutions which are characterized by an increasing number of oscillations in the cut-off region of the BJT or, equivalently, by an increasing number of pulses in the corresponding time series $x_3(t)$ (see Fig. 3). In the following, we will classify as an n-pulse solution a periodic solution exhibiting n pulses[4] (per period) in the waveform $x_3(t)$ or, equivalently, characterized by n oscillations in the cut-off

[4]More precisely, the number of pulses for $x_3(t)$ is defined as the number of intersections (per period) of the waveform with the axis $x_3 = 0$ (with $\dot{x}_3 < 0$).

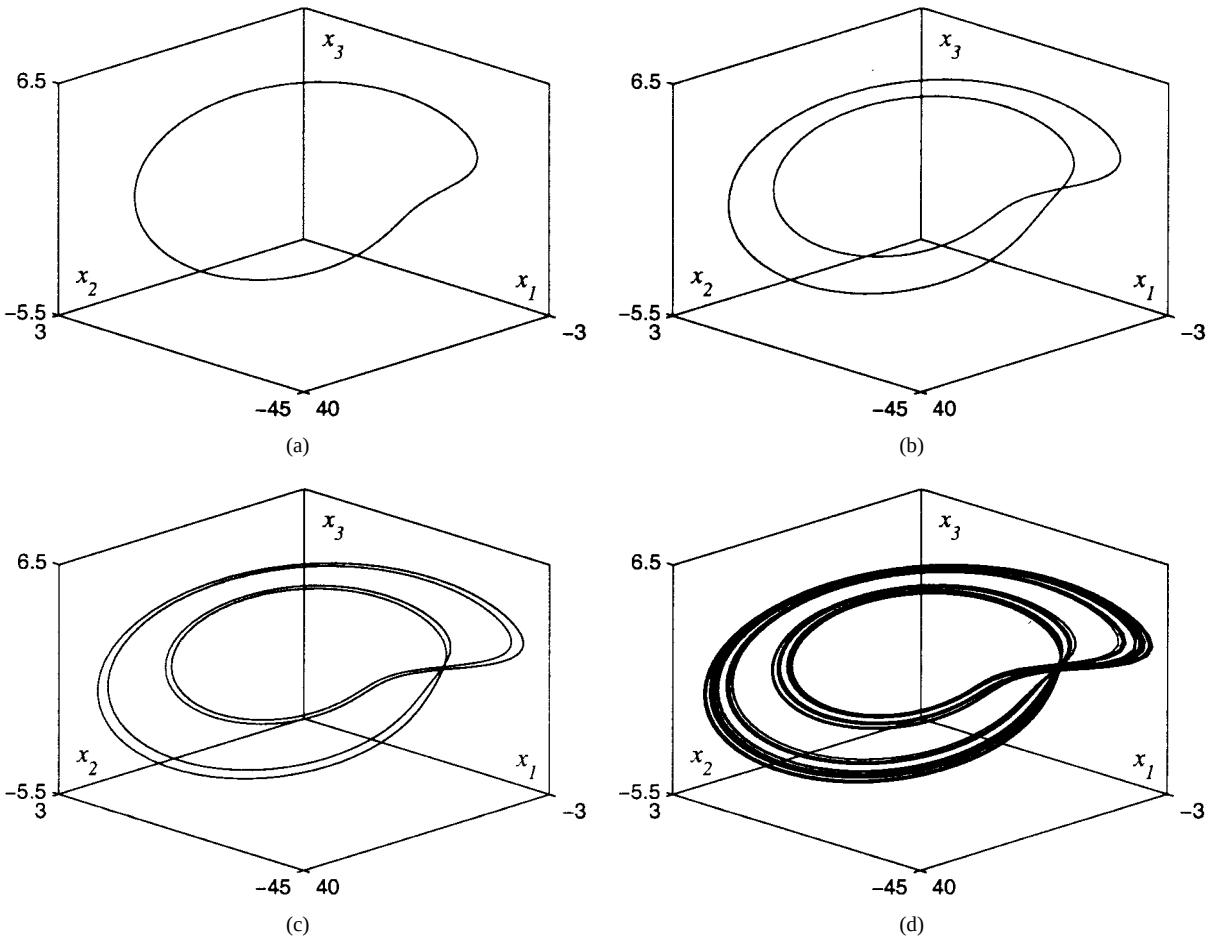

Fig. 5. Feigenbaum cascade of the nearly sinusoidal cycle. The parameter g^* is fixed at the value $\log_{10} g^* = 0.8800$ while Q is decreased through the bifurcations curves $F_{0,1}, F_{1,1}, \cdots F_{\infty,1}$ in Fig. 7. (a) Period-one orbit for $\log_{10} Q = 0.7500$. (b) Period-two orbit for $\log_{10} Q = 0.7296$. (c) Period-four orbit for $\log_{10} Q = 0.7026$. (d) Chaotic attractor for $\log_{10} Q = 0.6900$.

region. According to the definition above, the fundamental nearly-sinusoidal solution corresponds to a one-pulse solution.

It can be shown that the limit cycles associated with each periodic solution will undergo several bifurcations when varying the parameters. Namely, the following,

- *Flip* (or *period-doubling*) bifurcations when the cycle loses its stability and a cycle with double period appears instead.
- *Tangent* (or *fold*) bifurcations when two cycles with different stability properties collide and disappear;
- *Homoclinic* bifurcations, where a cycle collides with an equilibrium point, giving rise to a solution which is bi-asymptotic to the equilibrium point itself. When the equilibrium has a pair of complex eigenvalues the homoclinic bifurcation is said to be of the Shil'nikov type.

We emphasize that the invariants generated by the bifurcations described above exhibit similar geometrical features to the n-pulse solution from which they originated. In that sense, they can be considered part of the same family of solutions, i.e., relatives of the n-pulse solution.

This concept is illustrated in the case of a period-doubling sequence of bifurcations leading to a Feigenbaum-like strange attractor, as shown in Fig. 5. Similarly, Fig. 6(b) shows the Shil'nikov-type strange attractor associated with the homoclinic orbit for the nearly-sinusoidal solution reported in Fig. 6(a).

B. Bifurcation Diagram

Even though the bifurcation diagram for the Colpitts oscillator, with respect to the parameters Q and g^* is quite complex,[5] we will show how it can be decomposed in terms of simpler bifurcation structures. The overall structures can be exposed by identifying the bifurcation structures associated with each n-pulse solution.

1) Basic Bifurcation Structure: Fig. 7 reports the bifurcation structure corresponding to the one-pulse solution (i.e., the nearly-sinusoidal oscillation).

In Section VI-B.2, we will show that the generic n-pulse solution admits an almost identical bifurcation structure. Thus, in the following, even if Fig. 7 refers to the one-pulse solution, we will refer to it as the bifurcation structure associated with the generic n-pulse solution.

The notation system adopted henceforth for the single, n, and double (q, n) subscripts, will be such that the index n refers to the solution family (n pulse), while the index q is used

[5] A detailed description of the bifurcation diagram is beyond the scope of this paper. It will be published elsewhere.

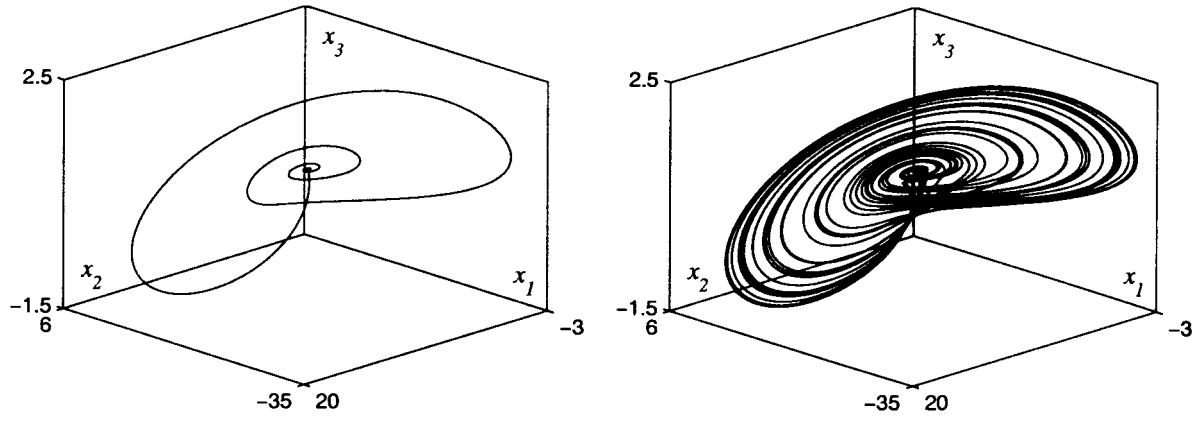

Fig. 6. Shil'nikov chaos. (a) Shil'nikov homoclinic orbit for $\log_{10} Q = 0.1502$ and $\log_{10} g^* = 0.5000$. (b) Associated chaotic attractor for $\log_{10} Q = 0.1510$ and $\log_{10} g^* = 0.5000$.

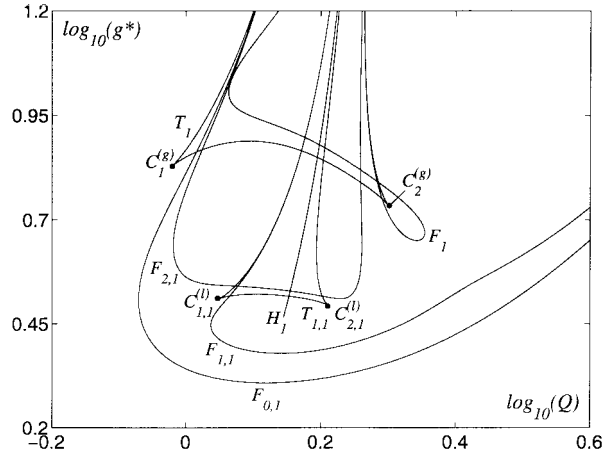

Fig. 7. Bifurcation diagram of the nearly sinusoidal (one-pulse) solution family. The symbols F, T, and H, denote flip, tangent, and homoclinic bifurcations, respectively. The points $C_{1,1}^{(l)}$, $C_{2,1}^{(l)}$, and $C_1^{(g)}$, $C_2^{(g)}$ are cusp codimension-two bifurcation points and imply local (l) and global (g) coexistence, respectively. The notations adopted for the single, n, and double (q, n) subscripts, are such that the index n refers to the solution family (n pulse), while the index q is used for enumeration purposes within the same kind of bifurcation. The bifurcation diagram shown can be considered also as the basic bifurcation structure associated with the generic n-pulse solution family.

for enumeration purposes in the case of multiple occurrences of the same type of bifurcation.

Substructure I: Homoclinic Bifurcation Structure

The first substructure we discuss is that associated with the Shil'nikov homoclinic bifurcation (curve H_1 in Fig. 7).

The bifurcations associated with a homoclinic bifurcation have been completely characterized theoretically [20], [21]. Namely, the scenario includes an infinity of flip and tangent bifurcations accumulating toward the homoclinic locus H_1. Moreover, each tangent bifurcation curve admits two points of cusp degeneracy. For the sake of clarity, in Fig 7 we reported only the first two flip bifurcations ($F_{1,1}$ and $F_{2,1}$) and the first tangent ($T_{1,1}$) bifurcation, respectively. As can be seen from Fig. 7, the latter admits two cusp degeneracy points ($C_{1,1}^{(l)}$ and $C_{2,1}^{(l)}$).

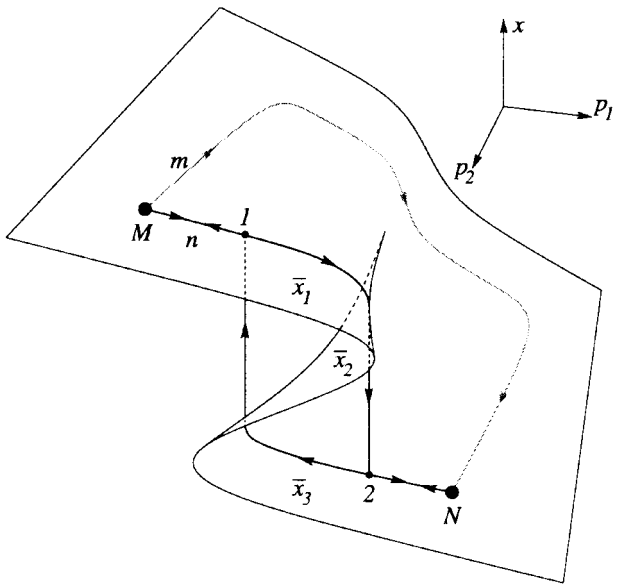

Fig. 8. Sketch of the folding of the invariant manifold at a cusp bifurcation. Here p_1 and p_2 are two generic control parameters, while x is the state space. The surface represents how the system invariants depend upon the parameters. Outside the cusp region there is only one invariant (for instance a cycle). Inside the cusp region there are three different coexisting invariants. The outer invariants have opposite stability properties with respect to the middle one. For instance the outer ($\overline{x}_1$ and $\overline{x}_3$) are stable (attractors) and the middle one ($\overline{x}_2$) is a saddle. Because of the folding of the invariant manifold, a change in the parameters can give rise to different effects. Namely, by moving the parameters from $\boldsymbol{M}$ to $\boldsymbol{N}$ along path m, the corresponding attractor is deformed smoothly. On the other hand, hysteretic phenomena associated with a sudden (catastrophic) change of attractor are observed when moving the parameters along the path n.

A cusp degeneracy occurs when three invariants (cycles) collide and disappear. This degenerate situation is illustrated in Fig. 8, where the geometry of the corresponding cycle manifold is shown. Here, p_1 and p_2 indicate two generic control parameters, while x represents some measure of the solution. From Fig. 8 it is evident that following the path m the solution varies smoothly, while by varying the parameters along the path n a typical hysteretic cycle is observed. We remark that the presence of hysteresis implies the coexistence of different (stable) solutions locally, near the cusp point.

For the model of the Colpitts oscillator, we expect coexistence of solutions and, thus, hysteretic behavior when varying a parameter forward and backward transversely to the tangent bifurcation curve $(T_{1,1})$ near the cusp points. We refer to this situation as a local (l) coexistence (in contrast with the global one discussed later) associated with Shil'nikov homoclinic bifurcations.

Having identified the homoclinic scenario allows us to exploit the theory for classifying the type of attractor, depending on the parameters values. In particular, we can use the first flip and tangent bifurcations to bound the regions with different dynamical behavior. The theory [21] predicts that, for instance, the area enclosed between the curves $F_{1,1}$ and $F_{2,1}$ is characterized by a (one-pulse) Feigenbaum strange attractor [see Fig. 5(d)]. On the other hand, the region within the curve $T_{1,1}$ corresponds to a (one-pulse) Shil'nikov type chaotic attractor [see Fig. 6(b)]. Finally, the remaining area within $F_{0,1}$ is characterized by the existence of subharmonics of the one-pulse solution, due to the period-doubling cascade opened by $F_{0,1}$.

Substructure II

We now discuss the other bifurcation substructure which is visible in Fig. 7, namely, the one comprising the two bifurcations curves T_1 and F_1 corresponding to tangent and flip bifurcations, respectively. In contrast to the previous one, this structure is not implied by the theory of homoclinic systems and its existence should be seen as a peculiarity of this system, even though it is a relatively common structure [22], [23].

We emphasize that the substructure described above organizes the coexistence of (two or more) attractors belonging to *different* solution families. In fact, as discussed in detail in the next section, for some regions of the parameter space the bifurcation structures associated with different solution families may overlap. In such regions, two or more attractors coexist. This coexistence can be observed for example at the cusp degeneracy points $C_1^{(g)}$ and $C_2^{(g)}$. The situation is similar to that previously described for cusp bifurcations (see Fig. 8). However, in this case, on the two floors of the cycle manifold there exist solutions belonging to different families. Because this coexistence is not predicted by any local theory, we refer to it as a global (g) coexistence.

2) General Bifurcation Diagram: As already mentioned, we can generalize the results obtained for bifurcations of the one-pulse solution to the generic n-pulse solution family. Namely, it can be shown that the n-pulse solutions exhibit an almost identical bifurcation structure to that shown in Fig. 7 but, obviously, for different values of the parameters. Technically, the only difference is the fact that the bifurcations of the one-pulse solution are bounded by the curve $F_{0,1}$, which is a flip bifurcation while, for the remaining n-pulse $(n \geq 2)$ solutions, the corresponding bifurcation structures are bounded by tangent bifurcation curves $T_{0,n}$.

The situation is illustrated in Fig. 9. For clarity we show only the main bifurcation curves corresponding to the fundamental nearly-sinusoidal solution (cf., Fig. 7), the two- and three-pulse solutions. The self-similar structure exhibited by the bifurcation diagram reflects the fact that the different families of periodic solutions share the same basic bifurcation structure.

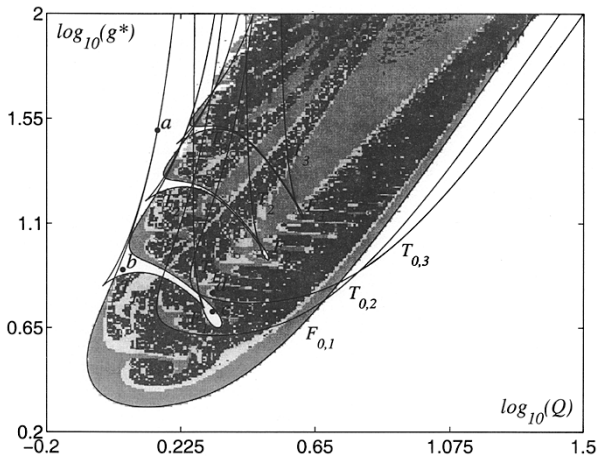

Fig. 9. Self-similar bifurcation structure superimposed on the simulation results [see also Fig. 4(a)] for comparison purposes. For each n-pulse periodic solution (with $n = 1, 2, 3$) we have shown only the outermost bifurcation curves $F_{0,1}, T_{0,n}$ and T_n, F_n, associated with substructures I and II, respectively.

C. Coexistence of Attractors

Summarizing, we have identified two possible types of coexistence of solutions within the complex bifurcation diagram of the Colpitts oscillator, namely, the following.

- Local coexistence, related to cusp bistabilities occurring near the homoclinic bifurcation loci in the parameter space.
- Global coexistence, meaning the multistabilities due to overlapping of the bifurcation structures associated with different families of periodic solutions.

A few relevant examples of coexisting attractors are reported in Fig. 10(a)–(d), corresponding to the points $\boldsymbol{a}, \boldsymbol{b}, \boldsymbol{c}$, and $\boldsymbol{d}$ in Fig. 9, respectively. In particular, Fig. 10(a) shows two coexisting limit cycles belonging to two different families of periodic solutions. In Fig. 10(b), a limit cycle coexisting with a chaotic attractor resulting from a Feigenbaum cascade are shown. Fig. 10(c) shows coexistence of a limit cycle and a chaotic attractor of the Shil'nikov type. Finally, in Fig. 10(d) we report the case of two coexisting chaotic attractors, of Feigenbaum and Shil'nikov type, respectively.

D. Comparison with Simulation

Fig. 9 shows the results of the bifurcation analysis superimposed on the simulation results, for comparison purposes. We emphasize the following.

1) Simulation failed to distinguish between the different bifurcation structures associated with different families of solutions.
2) Simulation did not reveal the bifurcation structures that are visible outside the grey area, such as the Feigenbaum cascades associated with $T_{0,2}$ and $T_{0,3}$ on the right-hand side and with T_1, T_2, and T_3, on the left-hand side. The fact that these solutions were not observed by simulation is related to their relatively small basins of attraction.
3) Finally, simulation is unlikely to detect coexisting attractors.

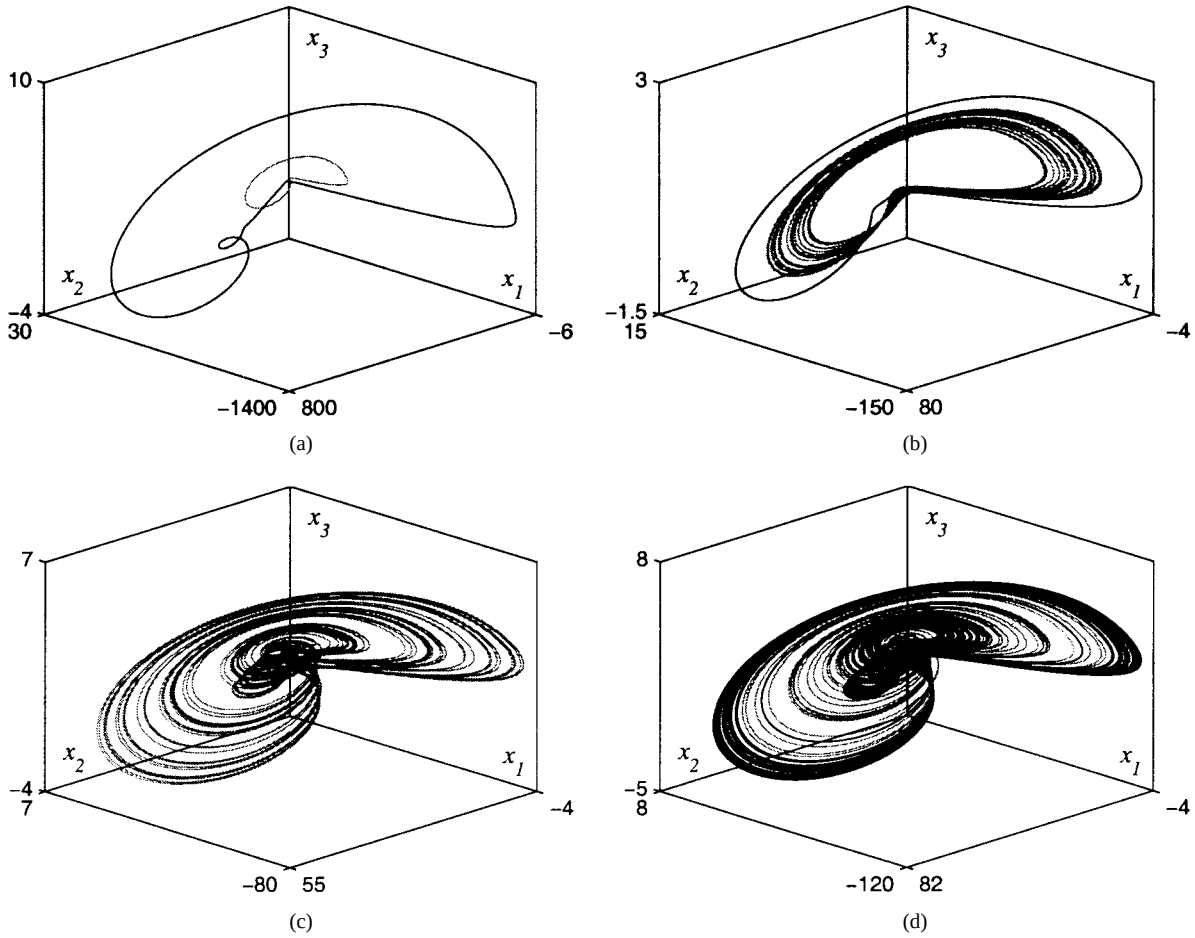

Fig. 10. Coexistence of attractors for the Colpitts oscillator at the points $\boldsymbol{a}, \boldsymbol{b}, \boldsymbol{c}$, and $\boldsymbol{d}$ of Fig. 9. (a) Coexistence of two different limit cycles for $\log_{10} Q = 0.1525$ and $\log_{10} g^* = 1.5000$. (b) Coexistence of limit cycle and Feigenbaum chaos for $\log_{10} Q = 0.0430$ and $\log_{10} g^* = 0.9000$. (c) Coexistence of limit cycle and Shil'nikov chaos for $\log_{10} Q = 0.3250$ and $\log_{10} g^* = 0.7200$. (d) Coexistence of Feigenbaum and Shil'nikov chaos for $\log_{10} Q = 0.3250$ and $\log_{10} g^* = 0.8000$.

VII. Verification of the Model

A robustness analysis of the circuit model has been carried out with respect to the hypotheses (H.1)–(H.3) introduced in Section II-A.

Most of the nonidealities neglected (on purpose) during the modeling process introduce only quantitative differences, but the qualitative behavior with respect to the parameters is maintained.

However, regarding (H.1) concerning the ideal bias circuit, we would like to point out the main differences related to the birth of the oscillation when considering a real current source which has finite output resistance. In particular, we consider the nonzero conductance G_0 in parallel with I_0, as shown in Fig. 1(a). In this case, the normalized state equations [cf., (3)] of the Colpitts oscillator become

$$\begin{pmatrix} \dot{x}_1 \\ \dot{x}_2 \\ \dot{x}_3 \end{pmatrix} = \begin{pmatrix} \dfrac{g^*}{Q(1-k)}[-\alpha_F n(x_2) + x_3] \\ \dfrac{g^*}{Qk}[(1-\alpha_F)n(x_2) + x_3] - Q_0(1-k)x_2 \\ -\dfrac{Qk(1-k)}{g^*}[x_1 + x_2] - \dfrac{1}{Q}x_3 \end{pmatrix} \tag{7}$$

where

$$n(x_2) = \exp(-x_2) - 1$$

and we have relaxed the hypothesis (H.3b) as well. We define

$$Q_0 = \omega_0 L G_0,$$

while g^*, Q, and k are defined as in Section II-A.

The new loop gain, g_0^*, for which the phase condition of the Barkhausen criterion is satisfied, is given (for values of α_F sufficiently close to unity) by

$$g_0^* \simeq \frac{g^*}{1 + (1-k)(Q_0/Q) + (1-k)^2 Q_0^2 (1 + Q/Q_0)}, \quad \alpha_F \to 1 \tag{8}$$

where $g_0^* \to g^*$ when $Q_0 \to 0$ ($\Leftrightarrow G_0 \to 0$).

The Barkhausen criterion for this circuit configuration is then satisfied for $g_0^* = 1$. In order to make a comparison with the ideal case ($G_0 = 0$), we now consider the locus where the Barkhausen criterion is satisfied in the original parameter space (Q, g^*) for a fixed value of Q_0. This situation is summarized in Fig. 11, where the Hopf bifurcation locus computed numer-

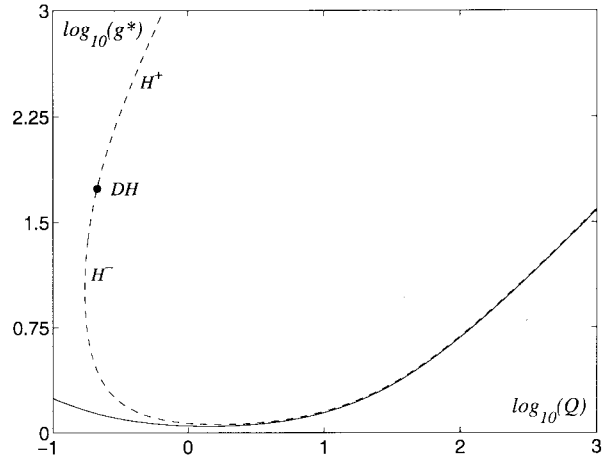

Fig. 11. Oscillation conditions for the model (7) in the plane (Q, g^*) for $k = 0.5$, $\alpha_F = 0.99$, and $Q_0 = 0.15$. The solid line is the oscillation condition provided by the Barkhausen criterion, while the dashed line corresponds to the actual Hopf bifurcation curve. The Hopf bifurcation is supercritical on the branch H^- and subcritical on the branch H^+. At the point DH the first Lyapunov coefficient l_1 goes to zero and the Hopf bifurcation is degenerate. Note that the Barkhausen criterion fails for low values of Q.

ically with CONTENT is also shown. As can be seen, in contrast to the ideal case, the Hopf bifurcation locus does not coincide entirely with the prediction of the Barkhausen criterion. In particular, note that the Barkhausen criterion (derived from a linear analysis) provides only necessary, but not sufficient, conditions for oscillation.

Finally, further investigations reveal that for low values of Q, the birth of the oscillation may be associated with a subcritical Hopf bifurcation, but this will be addressed elsewhere as it is beyond the scope of this paper.

VIII. DESIGN CONSIDERATIONS

Fig. 12 summarizes the results of our bifurcation analysis in a form that is suitable for design purposes. In particular, according to Section VI-B it is possible to identify regions in the parameter space characterized by the same (qualitative) dynamical behavior and bounded by well-defined bifurcation curves.

We note that a period-one orbit can be guaranteed by setting the control parameters, Q and g^* outside the domain D, corresponding to the nonlinear region in Fig. 12. Referring to Figs. 7 and 9, this domain D is bounded by the outermost curves $F_{0,1}$, $T_{0,2}, T_{0,3}$, and $T_{0,n}$ on the right-hand side and by the curves $F_{0,1}$ and T_1 on the left-hand side.

However, if a sinusoidal oscillation is required, we need to guarantee that the distortion of the signal generated does not exceed a certain threshold. For this reason, we have characterized the parameter space in terms of the THD[6] of the output signal $x_2(t)$. In particular, in Fig. 12 we show the isodistortion curves for values of THD lower than 1%. We note that, for low values of Q, these curves converge toward the line at $\log_{10} g^* = 0$ $(\Leftrightarrow g^* = 1)$ where the Barkhausen

[6]Recall that the THD of a waveform is defined as the ratio of the root-mean-square (rms) amplitude of the sum of the upper harmonics to the amplitude of the fundamental.

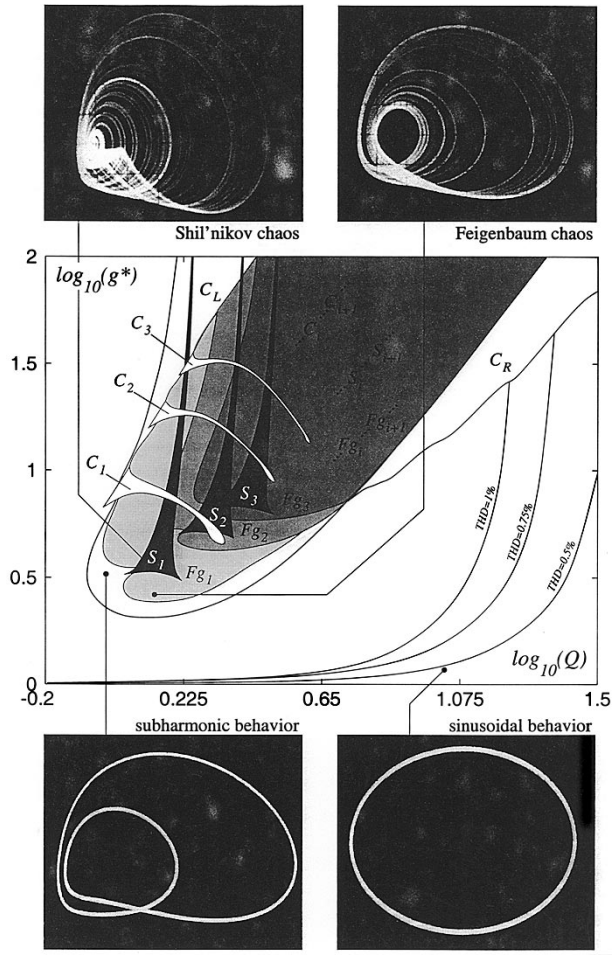

Fig. 12. Simplified bifurcation diagram for design applications. The white regions correspond to one-pulse behavior. We can assume the oscillation to be sinusoidal below the isodistortion line at $\mathrm{THD} = 1\%$. Thus, the latter separates the nearly-sinusoidal region from the nonlinear region. The gray regions are characterized by more complex behavior. Namely, in the regions Fg_n and S_n the system exhibits n-pulse Feigenbaum and Shil'nikov chaos, respectively. The cusp regions C_n are characterized by coexistence of the one-pulse solution with one or more attractors belonging to different solution families. The former is more likely to be observed because of its larger basin of attraction. For the same reason, the two outer regions labeled C_L and C_R have been colored white. We also show experimental oscillographs (in the (I_L, V_{C_2}) plane) for four representative points illustrating the main types of behavior exhibited by the Colpitts oscillator.

criterion is satisfied. Conversely, for higher values of Q the region of nearly sinusoidal behavior extends to relatively high values of g^*, as can be seen in Fig. 12. This is not surprising because if the quality factor is high enough, the loop gain can be increased without significant distortion.

On the other hand, from the point of view of chaos generation we have found that, in contrast to what had been hypothesized originally, homoclinic bifurcations are not the main sources of chaos in the Colpitts oscillator. In fact, Shil'nikov chaos is present only in narrow bands around the homoclinic loci H_n, while most of the chaotic regions that are visible in Fig. 4 are related to Feigenbaum cascades.

From an application point of view, in order to produce a robust chaotic oscillation Feigenbaum regions (Fg_n) are preferable to Shil'nikov regions (S_n) because the latter are

characterized by so-called Newhouse regions [24] which make the system extremely sensitive to parameter variations.

Also, the designer should be aware of the possible coexistence of periodic solutions for the Colpitts oscillator. This could be a global phenomenon, as at the cusp points denoted by C_i in Fig. 12, or local coexistence as described in the previous section.

Finally, Fig. 12 shows experimentally observed Lissajous figures for a practical implementation of the Colpitts oscillator [8], illustrating the main types of behavior analyzed in this paper.

IX. Conclusions

In this work we have shown how bifurcation analysis and continuation techniques can be exploited in a systematic way for designing both sinusoidal and chaotic oscillators. In addition, we have emphasized that results of simulations are often incomplete and thus should be treated with caution by a circuit designer. We have summarized our results with a parameter space design chart.

References

[1] A. I. Mees and L. Chua, "The Hopf bifurcation theorem and its applications to nonlinear oscillations in circuits and systems," *IEEE Trans. Circuits Syst.*, vol. 26, pp. 235–254, Apr. 1979.

[2] M. Basso, R. Genesio, and A. Tesi, "A frequency method for predicting limit cycle bifurcations," *Nonlinear Dynamics*, vol. 13, pp. 339–360, 1997.

[3] R. Genesio and A. Tesi, "A harmonic balance approach for chaos prediction: Chua's circuit," *Int. J. Bifurcation Chaos*, vol. 2, no. 1, pp. 61–79, 1992.

[4] M. Gilli and G. M. Maggio, "Predicting chaos through an harmonic balance technique: An application to the Time-Delayed Chua's Circuit," *IEEE Trans. Circuits Syst. I*, vol. 43, pp. 872–874, Oct. 1996.

[5] L. O. Chua, "The genesis of Chua's circuit," *Archiv Fuer Elektronik und Uebertragungstechnik*, vol. 46, no. 4, pp. 250–257, 1992.

[6] E. Freire, E. Ponce, and F. Torres, "Hopf bifurcations in piecewise linear planar dynamical systems," in *Proc. NDES'96*, Seville, Spain, June 1996, pp. 129–134.

[7] H. Kawakami and R. Lozi, Structure and Bifurcations of Dynamical Systems. Singapore: World Scientific, 1992.

[8] M. P. Kennedy, "Chaos in the Colpitts oscillator," *IEEE Trans. Circuits Syst. I*, vol. 41, pp. 771–774, Nov. 1994.

[9] C. Wegener, G. M. Maggio, and M. P. Kennedy, "An approximate one-dimensional model for the chaotic Colpitts oscillator," in *Proc. NDES'96*, Seville, Spain, June 1996, pp. 275–278.

[10] G. M. Maggio, C. Kennedy, and M. P. Kennedy, "Experimental manifestations of chaos in the Colpitts oscillator," in *Proc. ISSC'97*, Derry, Ireland, June 1997, pp. 235–242.

[11] S. H. Strogatz, Nonlinear Dynamics and Chaos: With Applications in Physics, Biology, Chemistry, and Engineering. New York: Addison-Wesley, 1994.

[12] W. Jansen, *CANDYS/QA: Algorithms, Programs, and User's Manual*, Univ. Potsdam, Dec. 1995.

[13] J. Millman and A. Grabel, *Microelectronics*, 2nd ed. Singapore: McGraw-Hill, 1988.

[14] G. M. Maggio and M. P. Kennedy, "On the relationship between continuous-time and discrete-time models of the Colpitts oscillator," in *Proc. NDES'97*, Moscow, Russia, 1997, pp. 240–245.

[15] E. Doedel, H.B. Keller, and J.P. Kernévez, "Numerical analysis and control of bifurcation problems (I) bifurcation in finite dimension," *Int. J. Bifurcation Chaos*, vol. 1, no. 3, pp. 493–520, 1991.

[16] A. R. Champneys and Y. A. Kuznetsov, "Numerical detection and continuation of codimension-2 homoclinic bifurcations," *Int. J. Bifurcation Chaos*, vol. 4, no. 4, pp. 785–822, 1994.

[17] Y. A. Kuznetsov, *Elements of Applied Bifurcation Theory*. New York: Springer-Verlag, 1995.

[18] E. Doedel and J. Kernévez, "AUTO: Software for continuation problems in ordinary differential equations with applications," *Applied Math.*, 1986.

[19] Y. A. Kuznetsov and V. V. Levitin, "CONTENT: A multiplatform environment for continuation and bifurcation analysis of dynamical systems," Centrum voor Wiskunde en Informatica, Kruislaan 413, 1098 SJ Amsterdam, The Netherlands, 1997.

[20] P. Glendinning and C. Sparrow, "Local and global behavior near homoclinic orbits," *J. Stat. Phys.*, vol. 35, nos. 5/6, pp. 645–696, 1984.

[21] P. Gaspard, R. Kapral, and G. Nicolis "Bifurcation phenomena near homoclinic systems: A two parameter analysis," *J. Stat. Phys.*, vol. 35, pp. 697–727, 1984.

[22] J. P. Carcasses, "Determination of different configurations of fold and flip bifurcation curves of a one or two-dimensional map," *Int. J. Bifurcation Chaos*, vol. 3, no. 4, pp. 869–902, 1993.

[23] A. P. Kuznetsov, S. P. Kuznetsov, I. R. Sataev, and L. O. Chua, "Two-parameter study of transition to chaos in Chua's circuit: Renormalization group, universality and scaling," *Int. J. Bifurcation Chaos*, vol. 3, no. 4, pp. 943–962, 1993.

[24] S. E. Newhouse, "The abundance of wild hyperbolic sets and nonsmooth sets for diffeomorphisms," *Publ. Math.*, IHES 50, pp. 101–151, 1979.

Gian Mario Maggio (S'95) received a Five-Year Honors degree in electronic engineering from the Politecnico di Torino, Turin, Italy, in March 1995 and the Ph.D. degree in electronic engineering from University College, Dublin, Ireland, in 1999. He carried out his graduation project on semiconductor modeling at Trinity College Dublin (Ireland).

During the summer of 1995 he worked as an electronic designer in the research and development laboratory of Philips Video Monza, Milan, Italy. He also worked on harmonic balance methods at the Politecnico di Torino, Turin, Italy. He has visited the Swiss Federal Institute of Technology, Lausanne (EPFL), the University of Bristol, and the University of California, Berkeley. He has been appointed a Postdoctoral Fellow at the Institute of Nonlinear Science (INLS), the University of California, San Diego. His research interests are in the area of analog design, solid state devices, nonlinear dynamics of electronic circuits (especially oscillators), and chaos generation.

Dr. Maggio was the recipient of a Marie Curie fellowship.

Oscar De Feo received the Bachelor degree (*Laude*) in industrial electronics in 1990 from the Maxwell High School, Milan, Italy, and the Five-Year degree (*Laude*) in Computer Science Engineering from the Politecnico di Milano, Milan, Italy, in 1995. In January 1997 he joined the Chair of Circuits and Systems at the Swiss Federal Institute of Technology, Lausanne, Switzerland, where he is working toward the Ph.D. degree.

He was with the Fondazione Eni Enrico Mattei (FEEM), Milan, Italy, as a Postgraduate Fellow, working on problems of sustainable development and environmental impact. He continued his research studies in nonlinear dynamics participating in the Young Scientists' Summer Program (YSSP) at the International Institute for Applied Systems Analysis (IIASA), Laxenburg, Austria. During 1997 and 1998 he held visiting research positions at the IIASA, at the Research Institute for Mathematics and Computer Science (CWI) Amsterdam, The Netherlands, and at the Department of Electronic and Electrical Engineering, University College, Dublin, Ireland. Oscar's research interests are in the fields of bifurcation and nonlinear systems theory, numerical methods for nonlinear system analysis, bioengineering and design of nonlinear systems for engineering.

Mr. De Feo received the Mikhalevich Award for his research activities.

Michael Peter Kennedy (S'84–M'91–SM'95–F'98) received the B.E. degree in electronics from the National University of Ireland in 1984, and the M.S. and Ph.D. degrees from the University of California, in 1987 and 1991, respectively,

He has worked as a Design Engineer with Philips Electronics, a Postdoctoral Research Engineer at the Electronics Research Laboratory, University of California, Berkeley, and as a Professeur Invité at the EPFL, Switzerland. He returned to University College Dublin (UCD) in 1992 as a College Lecturer in the Department of Electronic and Electrical Engineering, where he teaches electronic circuits and computer-aided circuit analysis, and directs the undergraduate Electronics Laboratory. He was appointed Senior Lecturer at UCD in 1996. He has published over 100 articles in the area of nonlinear circuits and has taught courses on nonlinear dynamics and chaos in England, Switzerland, Italy, and Hungary. He has held visiting research positions at the EPFL, AGH Kraków, TU Budapest, and the University of California, Berkeley. His research interests are in the analysis, design and simulation of nonlinear dynamical systems for applications in communications, and signal processing.

Dr. Kennedy received the 1991 Best Paper Award from the *International Journal of Circuit Theory and Applications*. He served as an Associate Editor of the IEEE TRANSACTIONS ON CIRCUITS AND SYSTEMS from 1993 to 1995, Guest Editor of 1997 and 1999 special issues in the IEEE TRANSACTIONS ON CIRCUIT AND SYSTEMS, and was Chairman of the IEEE Technical Committee on Nonlinear Circuits and Systems from 1998 to 1999.